ARTICLE

Molecular and cellular mechanisms for differential effects of chronic social isolation stress in males and females

Zi-Jun Wang[1], Treefa Shwani[1], Junting Liu[2], Ping Zhong[1], Fengwei Yang[1], Kelcie Schatz[1], Freddy Zhang[1], Arnd Pralle[2] and Zhen Yan[1]✉

Chronic social isolation stress during adolescence induces susceptibility for neuropsychiatric disorders. Here we show that 5-week post-weaning isolation stress induces sex-specific behavioral abnormalities and neuronal activity changes in the prefrontal cortex (PFC), basal lateral amygdala (BLA), and ventral tegmental area (VTA). Chemogenetic manipulation, optogenetic recording, and in vivo calcium imaging identify that the PFC to BLA pathway is causally linked to heightened aggression in stressed males, and the PFC to VTA pathway is causally linked to social withdrawal in stressed females. Isolation stress induces genome-wide transcriptional alterations in a region-specific manner. Particularly, the upregulated genes in BLA of stressed males are under the control of activated transcription factor CREB, and CREB inhibition in BLA normalizes gene expression and reverses aggressive behaviors. On the other hand, neuropeptide *Hcrt* (Hypocretin/Orexin) is among the top-ranking downregulated genes in VTA of stressed females, and Orexin-A treatment rescues social withdrawal. These results have revealed molecular mechanisms and potential therapeutic targets for stress-related mental illness.

Molecular Psychiatry (2022) 27:3056–3068; https://doi.org/10.1038/s41380-022-01574-y

INTRODUCTION

Brain function is significantly affected by genetic disturbances and environmental experiences. Chronic stress, a prominent environmental factor, induces profound and long-lasting maladaptation, precipitating the development of neuropsychiatric disorders, including anxiety and depression [1, 2]. One important but understudied phenomenon is that significant sex differences exist in stress-associated diseases [1]. For example, the prevalence of aggression/violence is significantly higher in men [3], while women are more vulnerable to develop depression [4, 5] and post-traumatic stress disorder [6, 7].

Adolescence represents a critical developmental stage when the maturation of brain network occurs, such as the glutamatergic and dopaminergic systems in the prefrontal cortex (PFC) [8] and mesolimbic regions [9, 10]. Therefore, it is a particularly vulnerable period during which chronic stress induces susceptibility for mental disorders [11, 12]. People exposed to early life stress have heightened vulnerability to mood and anxiety disorders [11]. Animals with early life stress exhibit a series of behavioral abnormalities, such as aggression [13, 14], anxiety [15], social withdrawal [14, 16, 17], and learning deficits [18]. One potent stressor is social isolation during adolescence, which alters key brain regions involved in emotional control, such as PFC (prelimbic cortex, infralimbic cortex, and anterior cingulate cortex), basal lateral amygdala (BLA), and ventral tegmental area (VTA) [14, 17, 19–22], and induces detrimental effects on mental health [10, 11, 22].

In this study, we sought to reveal neurobiological mechanisms underlying sex-specific effects of chronic adolescent isolation stress. We used chemogenetics, optogenetics, and in vivo recordings of calcium signal in behaving mice to dissect out specific brain regions and pathways that play a causal role in controlling the behavioral outcomes in stressed males and females. We also performed transcriptomic studies to determine the role of region-specific dysregulation of gene expression in behavioral manifestations by isolation stress.

RESULTS

Adolescent social isolation stress induces heightened aggression in males, which is linked to the altered PFC to BLA pathway

Social isolation stress is commonly used as a model for studying the neurobiological underpinning of psychiatric disorders precipitated by early life stress [14, 16, 17, 20, 23]. Thus, we first performed multiple behavioral assays [24–26] to examined the effects of 5-week post-weaning isolation stress. In the resident-intruder (RI) assay, socially-isolated (SI) males exhibited a significant increase of aggressive behaviors toward intruders, compared to group-housed (GH) control males, consistent with previous findings [13], while SI female mice did not show elevated aggression (Fig. 1A). In the elevated plus maze (EPM) test, SI mice of both sexes spent less time on the open arm and more time on the closed arm (Fig. S1A), suggesting the elevated anxiety phenotype [15]; however, no significant changes were found in the open-field test (Fig. S1B). In the test of sensorimotor gating function that suppresses excessive behavioral responses to

[1]Department of Physiology and Biophysics, School of Medicine and Biomedical Sciences, State University of New York at Buffalo, Buffalo, NY, USA. [2]Department of Physics, College of Arts and Sciences, State University of New York at Buffalo, Buffalo, NY, USA. ✉email: zhenyan@buffalo.edu

Received: 12 October 2021 Revised: 6 April 2022 Accepted: 8 April 2022
Published online: 21 April 2022

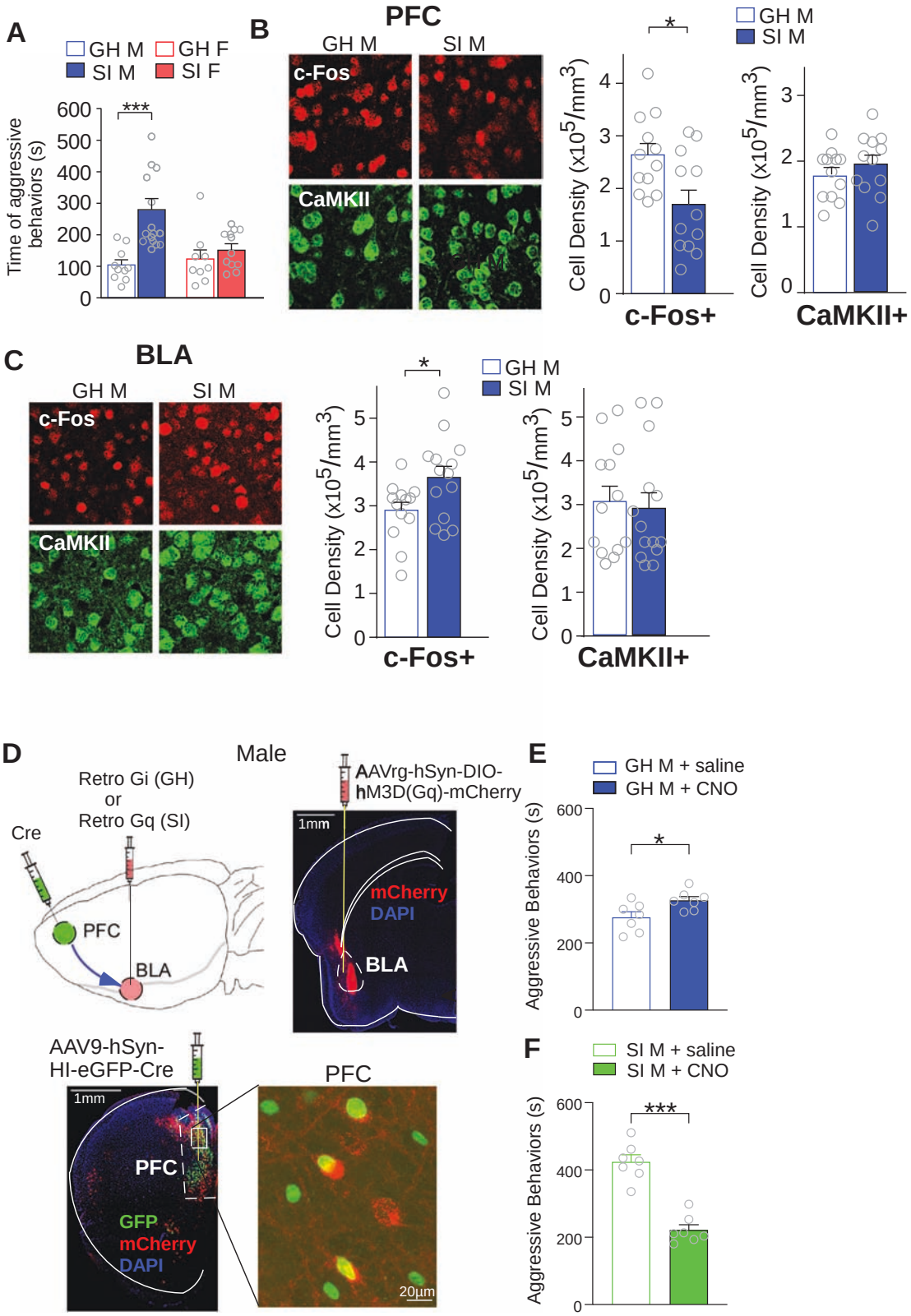

disruptive stimuli, pre-pulse inhibition (PPI) of acoustic startle was significantly reduced in both male and female SI mice without the change on the startle response (Fig. S1C).

With the elevated aggression exhibited selectively in SI males, we next examined the underlying circuitry mechanisms. It has been postulated that impulsive aggression and violence arise as a consequence of faulty emotion regulation by the complex circuit consisting of frontal cortex, amygdala, and several other interconnected regions [27], so we used c-Fos expression, a measure of neuronal activity, to examine changes in PFC and BLA

Fig. 1 Elevated aggression in socially-isolated (SI) males is linked to the altered PFC to BLA pathway. A Bar graphs showing the time of aggressive behavior in the RI test of GH and SI of both sexes ($n = 9$–15/group, $F_{1,36(stress)} = 13.35$, $p < 0.001$; two-way ANOVA). **B**, **C** Confocal images and quantification of immunostaining of c-Fos (red), CaMKII (green) and DAPI (blue) in the PFC (**B**) or BLA (**C**) of GH and SI males (**B** $n =$ 12 slice/4 mice/group, $t_{22} = 2.74$, $p < 0.05$, t test; **C** $n = 10$–14 slice/4 mice/group, $t_{25} = 2.36$, $^*P < 0.05$, t test). **D** Diagram and images showing the location and expression of the stereotaxically-injected GFP-Cre AAV to medial PFC and retrograde DIO-DREADD-mCherry AAV to male BLA. hM4D(Gi) DREADD was injected to GH males, while hM3D(Gq) DREADD was injected to SI males. The zoomed-in images of PFC show mCherry signals in GFP+ neurons, indicating that DREADD AAV is retro-transported from BLA to PFC. **E** Bar graphs showing the time of aggressive behaviors in RI tests of GH males injected with saline or CNO to inhibit PFC → BLA pathway ($n = 7$/group, $t_{11} = 2.57$, $p < 0.05$, t test). **F** Bar graphs showing the time of aggressive behaviors in RI tests of SI males injected with saline or CNO to activate PFC → BLA pathway ($n =$ 7/group, $t_{11} = 7.82$, $p < 0.001$, t test). Data are presented as mean ± SEM. In all figures: $^*p < 0.05$; $^{**}p < 0.01$; $^{***}p < 0.001$.

of stressed animals. We found a significantly reduced number of c-Fos-positive PFC neurons, but not a total number of PFC pyramidal neurons (CaMKII-positive), in SI males (Fig. 1B). The number of c-Fos-positive neurons in BLA, but not the total number of BLA principal neurons (CaMKII-positive), was significantly increased in SI males (Fig. 1C), while c-Fos-positive neurons were unchanged in BLA of SI females (Fig. S2A). To complement c-Fos studies, we stained with another neuronal activity marker Egr1. We found that chronic social isolation stress decreased Egr1 expression level in PFC of SI males (Fig. S2B), while elevated Egr1 expression in male BLA (Fig. S2C), but not female BLA (Fig. S2D). These data suggest that SI induces the dampening of PFC activity and the elevation of BLA activity in males.

PFC regulates emotional processes by top-down control of subcortical brain regions [8, 22, 28]. To determine whether the alteration of PFC to BLA pathway is causally linked to aggressive behaviors in SI males, we next used the chemogenetic tool DREADD to manipulate this specific pathway in a bi-directional manner. The GFP-tagged Cre virus was injected bilaterally to PFC, and the mCherry-tagged retrograde double floxed DREADD virus was injected into the BLA of male mice. Selective manipulation of the PFC to BLA pathway was achieved by the systemic administration of CNO (3 mg/kg, i.p.) [29]. To examine the sufficiency and necessity of PFC to BLA pathway in aggression, Gi DREADD was injected to BLA of GH males, and Gq DREADD was injected to BLA of SI males (Fig. 1D). We found that inhibiting PFC → BLA projection by CNO treatment in GH males induced aggression during RI tests (Fig. 1E), while activating PFC → BLA projection by CNO treatment in SI males significantly attenuated aggressive behaviors (Fig. 1F). These data have provided bi-directional evidence indicating that PFC to BLA pathway is causally linked to male aggression.

To investigate how the diminished activity of PFC projection neurons in stressed males affects the BLA, we injected the CaMKII promoter-driven, mCherry-tagged channelrhodopsin-2 (ChR2) into PFC, and recorded light-induced synaptic responses in BLA principal neurons of brain slices [30]. The expression of ChR2 in PFC pyramidal neurons and their terminals in BLA were confirmed (Fig. 2A), indicating that BLA principal neurons receive direct excitatory inputs from PFC. Stimulation of PFC terminals in BLA could also recruit local GABAergic interneurons to form disynaptic feedforward inhibition in BLA principal neurons [25, 28]. So we recorded inhibitory postsynaptic currents (IPSC) (holding at 0 mV) and excitatory postsynaptic currents (EPSC) (holding at −70 mV) evoked by brief pulses of blue light [30]. We found that the amplitude of opto-IPSC was significantly reduced in SI males (Fig. 2B). Moreover, the paired-pulse ratio (PPR) of opto-IPSC was significantly changed (Fig. 2C), suggesting a presynaptic mechanism underlying the reduction of synaptic inhibition in BLA principal neurons of SI males. Opto-EPSC was not altered (Fig. 2D), and IPSC/EPSC ratio was significantly reduced in SI males (Fig. 2E), indicating that PFC hypofunction switched E/I balance to over-excitation (disinhibition) in BLA principal neurons of SI males. In contrast, optogenetic recordings of GH vs. SI female mice found no significant differences in opto-IPSC (Fig. 2F), opto-EPSC (Fig. 2G), and IPSC/EPSC ratio (Fig. 2H). These data have revealed a specific change of PFC to BLA pathway in SI males: the diminished PFC function during stress leads to disinhibition of amygdala, which promotes hyperarousal and aggression.

Transcriptomic changes in BLA of stressed males underlie heightened aggression

The development and expression of aggressive behaviors are influenced by the complex interactions between genes, biological signals, neural circuits, and the environment [31]. To better understand how BLA, a key locus of emotional regulation [25, 32], is involved in stress-induced male aggression, we investigated transcriptomic changes in BLA of SI male mice. RNA-seq revealed 207 upregulated genes and 169 downregulated genes in BLA of SI males, compared to BLA of GH males (Fig. 3A, Supplementary Tables 1, 2). Heatmaps of the up- and downregulated DEGs showed that GH samples clustered separately from SI samples (Fig. 3B). Functional protein classification analysis indicated that many up- or downregulated genes were transcription regulators, enzymes, and signaling molecules (Fig. 3C). GO analysis indicated that the most enriched biological process of upregulated genes was "aggressive behavior" (Fig. 3D), while the downregulated genes were primarily involved in "limbic system development" (Fig. 3D).

We further performed gene set enrichment analysis (GSEA) to identify transcription factors that regulate the DEGs in BLA of SI males. We identified CREB as the top-ranking transcription factor highly associated with the upregulated genes (Fig. 3E). CREB, whose activity increases in response to various stimuli [33], regulates the transcription of numerous substrates, including stress-released peptide hormones, and is a master controller of emotional states [33–38]. We found that the level of phosphorylated CREB (p-CREB), the active form of CREB that has transcriptional effects, was significantly increased in the BLA of SI male mice (Fig. 3F). Furthermore, qPCR experiments confirmed that the expression of genes involved in GO process "aggressive behavior" (*Avp*, *Oxt*, and *Avpr1)* and additional CREB-dependent gene targets (*Pax7*, *Coro6*, and *Rnps1*) were significantly increased in the BLA of SI male mice (Fig. 3G), suggesting the critical role of CREB in gene upregulation in the BLA of males after social isolation stress. In addition, mRNA levels of *Avp*, *Oxt*, and *Avpr1* in BLA from SI females were similar to those from GH females (Fig. 3H), indicating that these molecular changes are specific to males.

To further determine whether the activated CREB in BLA of SI males is responsible for heightened aggression, we treated SI male mice with a CREB inhibitor, 666-15 [39, 40], and examined molecular and behavioral consequences. The CREB inhibitor was locally injected into the BLA bilaterally (1.6 mM, 0.5 µl/side) after 5 weeks of social isolation. Compared to vehicle treatment, 666-15 treatment significantly reduced p-CREB level in BLA principal neurons of SI male mice (Fig. 3I). Moreover, the expression of many SI stress-elevated and CREB-dependent genes, such as *Oxt*, *Pax7*, *Coro6* and *Rnps1*, was significantly lowered by 666-15 treatment in BLA of SI males (Fig. 3J). Behavioral assays also showed significantly attenuated aggression in 666-15-treated SI male mice (Fig. 3K). These data suggest that CREB in male BLA may serve as a therapeutic target for aggression-associated mental illnesses.

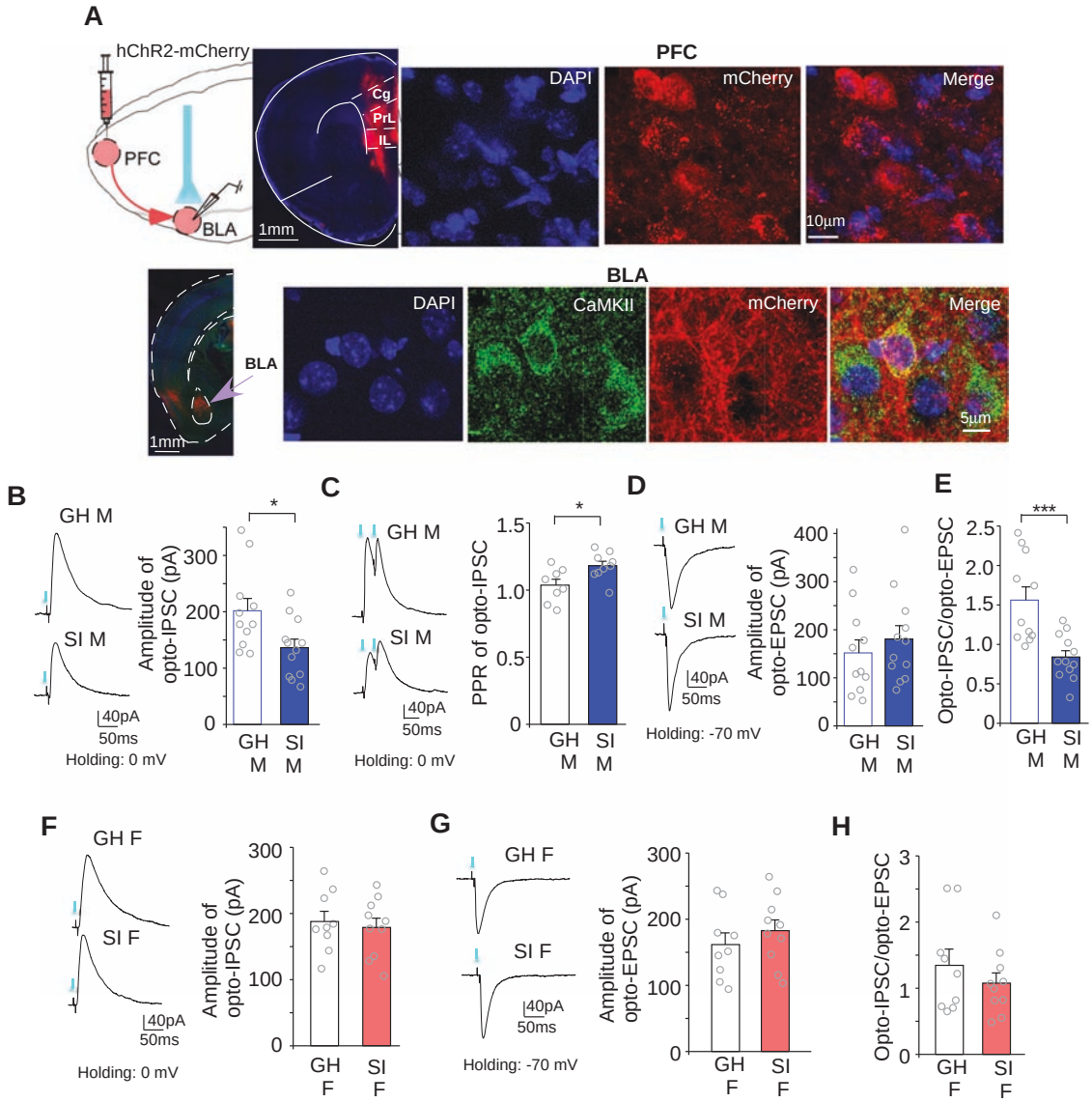

Fig. 2 Optogenetic recording shows the diminished feedforward inhibition in BLA principal neurons from PFC projections in stressed males. A A diagram of the experimental setting and confocal images showing the viral expression of ChR2(H134R)-mCherry in PFC (injection site) and ChR2-expressing terminals at the target region BLA. **B**, **D** Representative traces and quantification of inhibitory (**B**) or excitatory (**D**) postsynaptic currents evoked by the blue light pulse (5 ms) stimulation (opto-IPSC, opto-EPSC) in BLA principal neurons from GH and SI males ($n = 11$–12 cells/4 mice/group, opto-IPSC: $t_{21} = 2.49$, $p < 0.05$, t test). **C** Representative traces and quantification of paired-pulse ratio (PPR) of opto-IPSC evoked by two light pulses (40 ms Interval) in BLA principal neurons from GH and SI males ($n = 8$–9 cells/3 mice/group, $t_{15} = 2.62$, $p < 0.05$, t test). **E** The ratio of opto-IPSC/opto-EPSC amplitude in BLA principal neurons from GH and SI males ($t_{21} = 3.97$, $p < 0.001$, t test). **F**, **G** Representative traces and quantification of opto-IPSC and opto-EPSC in BLA principal neurons from GH and SI females ($n = 9$–10 cells/3 mice/group). **H** The ratio of opto-IPSC/opto-EPSC amplitude in BLA principal neurons from GH and SI females. Data are presented as mean ± SEM. In all figures: *$p < 0.05$; ***$p < 0.001$.

Adolescent social isolation stress induces social withdrawal in females, which is linked to the altered PFC to VTA pathway

While SI females did not show elevated aggression, they exhibited a social withdrawal phenotype, as indicated by significantly less time spent interacting with the social stimulus in the social approach (SA) assay than GH control females (Fig. 4A). In contrast, SI male mice had the similar social interaction time as GH control males (Fig. 4A).

To find out whether the diminished sociability in SI females is driven by the neuronal activity changes in PFC, a key region involved in social behaviors [8, 14, 41, 42], we performed in vivo calcium imaging of behaving animals. A fluorescent calcium indicator, GCaMP6s [43, 44], combined with fiber photometry, measured real-time neuronal activity fluctuations during social approach assays. GCaMP6s virus (AAV5-syn-FLEX- GCaMP6s) was injected into the PFC of female Exm1-Cre mice, which facilitated Cre-dependent GCaMP6s expression in pyramidal neurons. An optical fiber over the PFC allowed simultaneous delivery of 470 nm excitation light, 410 nm isosbestic light, and collection of GCaMP6s emission, which was recorded with a CMOS camera [43] (Fig. 4B).

First, mice were habituated in the testing chamber (containing an empty cup) for 30 min, and GCaMP6s fluorescence from the PFC was recorded for the last 5 min to obtain baseline calcium activity data. Reduced baseline calcium signal was observed in SI females, compared to GH controls (Fig. 4C). Averaging the baseline calcium activity over the population of animals (Fig. 4D) showed that SI females exhibit a significantly lower calcium

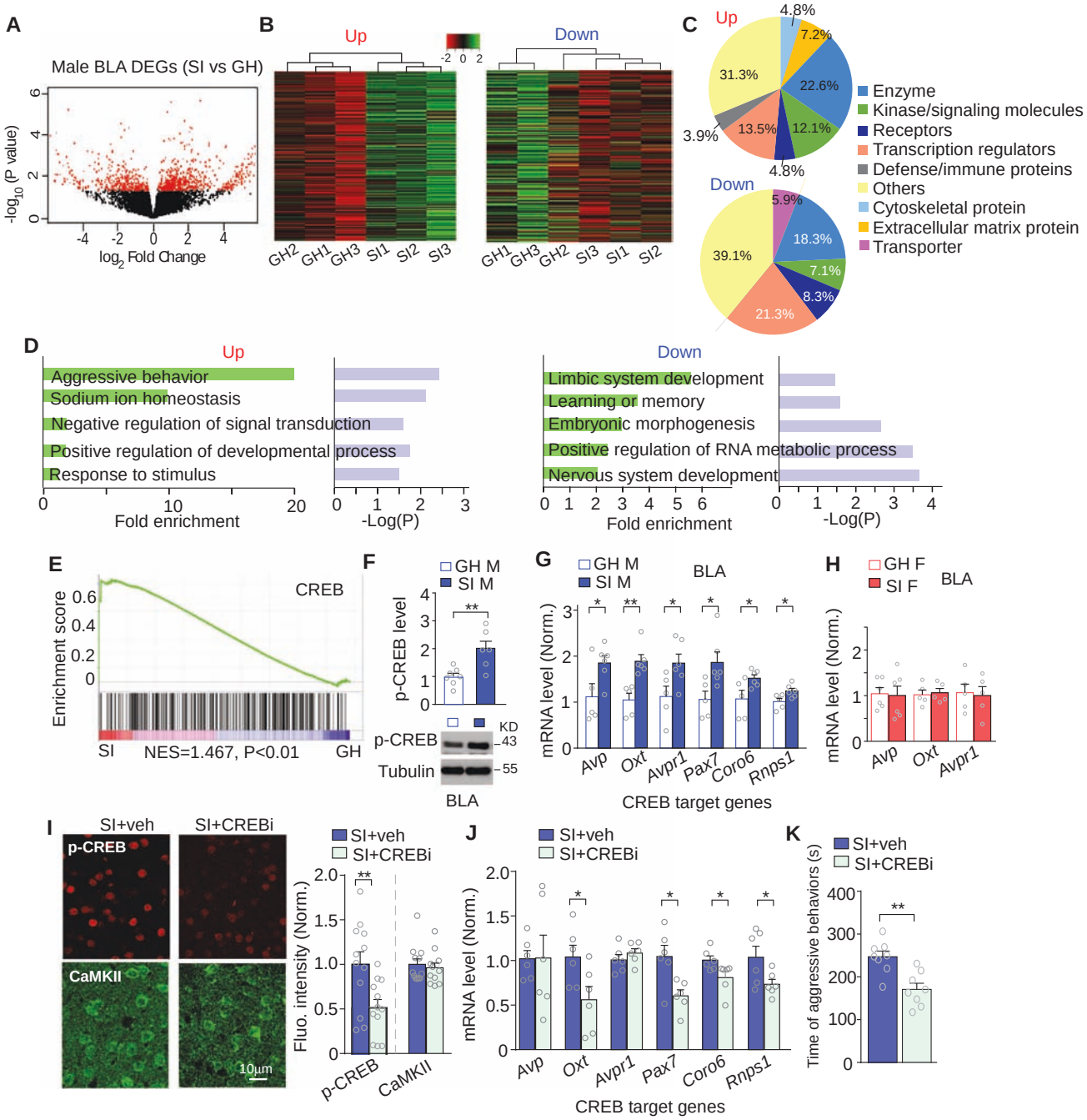

Fig. 3 Isolation stress-induced transcriptional changes in the BLA of male mice and aggressive behaviors are blocked by CREB inhibition. **A** Volcano plot of differentially expressed genes in the BLA of SI males, compared to GH males. **B** Heatmaps of up- and downregulated genes in BLA of SI males, compared to GH controls. **C** Functional protein classification for the up- and downregulated genes. **D** Enrichment analysis for the up- and downregulated genes. **E** GSEA analysis showing the positive correlation, as indicated by normalized enrichment score (NES), between the transcription factor CREB and the upregulated genes in BLA of SI mice (compared to GH controls). **F** Quantitation and representative immunoblots of p-CREB levels in BLA from GH and SI males ($n = 6$–7/group, $t_{11} = 3.40$, $p < 0.01$, t test). **G**, **H** The mRNA level of CREB target genes in BLA of GH and SI males (**G** $n = 5$–6/group, $p < 0.05$ or $p < 0.01$, t test) or BLA of GH and SI females (**H** $n = 5$–6/group). **I** Confocal images and quantification of immunohistochemical staining of p-CREB (red) and CaMKII (green) in the BLA of SI male mice treated with the CREB inhibitor 666-15 (stereotaxically injected to BLA) or vehicle ($n = 12$ slice from 3 mice/group, p-CREB: $t_{22} = 2.52$, $p < 0.05$, t test). **J** The mRNA level of CREB target genes in the BLA of SI male mice treated with 666-15 or vehicle ($n = 6$/group, $p < 0.05$, t test). **K** Bar graphs showing the time of aggressive behaviors in the RI tests of SI male mice treated with 666-15 or vehicle ($n = 8$/group, $t_{14} = 3.91$, $p < 0.01$, t test). Data are presented as mean ± SEM. In all figures: *$p < 0.05$; **$p < 0.01$; ***$p < 0.001$.

activity than GH controls in PFC pyramidal neurons (Fig. 4E). After placing the social stimulus (a sex- and age-matched control mouse) under the cup, the GH female exhibited a prominent increase of calcium signal during social interaction epochs (marked by red lines and indicated by the short distance of the test animal with the social stimulus). In contrast, the SI female did not show a significant rise of calcium activity above baseline during the shorter time engaged in social interaction (Fig. 4F). The peri-event averaged calcium signal showed that GH females had significantly increased activity in PFC pyramidal neurons,

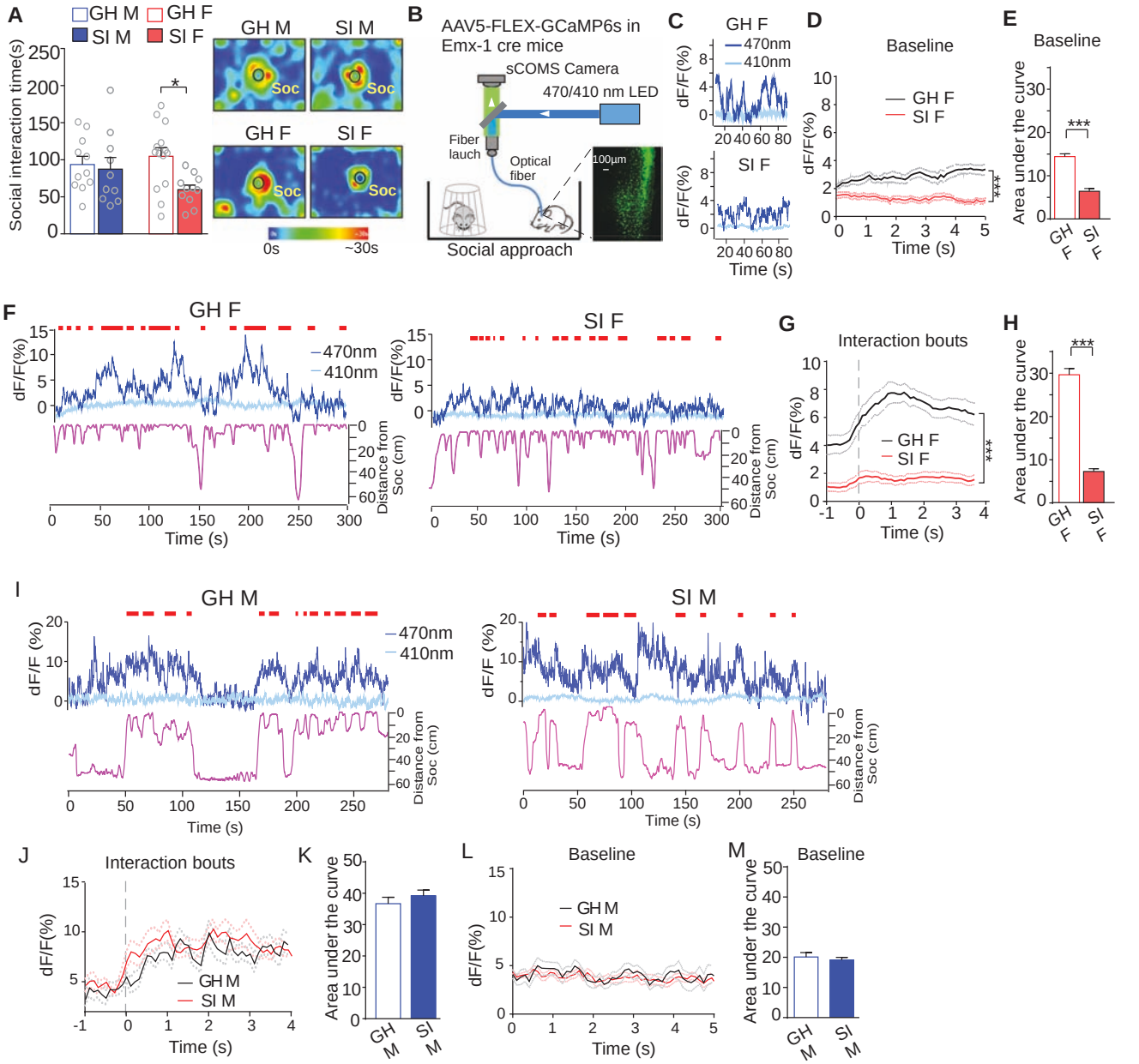

Fig. 4 In vivo calcium imaging shows the attenuated activation of PFC neurons by social stimuli in SI females. A Bar graph showing the social interaction time during the Social Approach (SA) test of GH and SI of both sexes ($n = 13$–16/group, $F_{1,42(stress)} = 4.86$, $p < 0.05$; two-way ANOVA). Insets: representative heatmaps illustrating the time spent in different locations in the chamber during social approach tests. Location of the social stimulus (Soc) is labeled by the circle. **B** Schematic of in vivo calcium imaging with fiber photometry. **C** Photometry traces from representative mice expressing GCaMP6s in the PFC during baseline recording of GH and SI females. dF/F represents the change in fluorescence from the median of the entire time series. **D** Peri-event plots of averaged calcium signals during baseline recording in GH and SI females ($n = 15$ bouts/3 mice/group, $F_{1,28(stress)} = 40.42$, $p < 0.001$, two-way ANOVA). **E** Bar graphs showing the integration under the curve of calcium signal in PFC during baseline recordings of GH and SI females ($t_{28} = 8.90$, $p < 0.001$, t test). **F** Photometry traces (top, blue) from representative GH and SI females expressing GCaMP6s in the PFC during the SA test. The distance between the testing mouse and the social stimulus during the SA test is also shown (pink, bottom). Red dashes: social interaction bouts from behavioral assays. **G** Peri-event plots of averaged calcium signals during social interaction bouts in GH and SI females ($n = 15$–17 bouts/3 mice/group, $F_{1,30(stress)} = 45$, $p < 0.001$, two-way ANOVA). **H** Bar graphs showing the calcium signal in PFC during SA tests of GH and SI females (H) ($t_{30} = 13.77$, $p < 0.001$, t test). **I** Photometry traces of GH and SI males expressing GCaMP6s in the PFC during SA test. **J**, **K** Peri-event plots and bar graphs of averaged calcium signals during social interaction bouts in GH and SI males ($n = 14$–15 bouts/3 mice/group, (**J**) $F_{1,27(stress)} = 1.54$, $p > 0.05$, two-way ANOVA; (**K**) $t_{27} = 2.64$, $p > 0.05$, t test). **L**, **M** Peri-event plots and bar graphs of averaged calcium signals during baseline recording of GH and SI males. Data are presented as mean ± SEM. In all figures: $^{**}p < 0.01$; $^{***}p < 0.001$.

beginning as soon as the social interaction started, while SI females failed to show the rise of calcium activity (Fig. 4G, H). Fiber photometry experiments in male mice indicated that GH and SI males exhibited a similar rise of calcium signal in PFC during social interaction (Fig. 4I–K), and a similar baseline calcium activity (Fig. 4L, M). These data have confirmed that isolation stress induces the loss of social interaction-coupled calcium increase specifically in PFC of SI females.

Next, we sought to find out the circuitry mechanisms that underlie the reduced sociability in SI females. In addition to PFC,

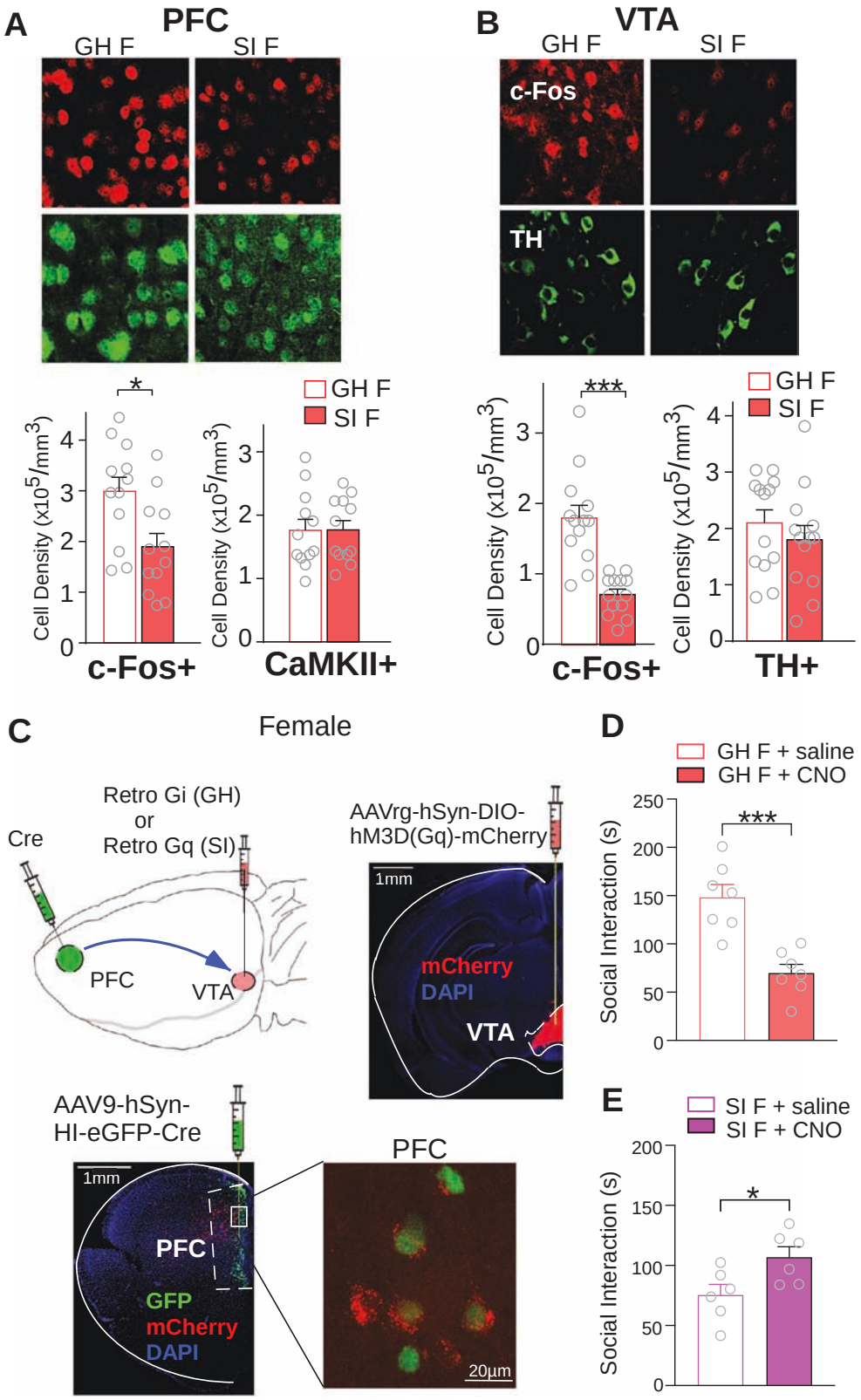

VTA is another region critically involved in regulating social behaviors [14, 21, 45–47]. Thus, we used the activity marker c-Fos to examine changes in PFC and VTA of stressed animals. We found a significantly reduced number of c-Fos-positive neurons in the PFC of SI females (Fig. 5A). The number of c-Fos-positive neurons in VTA was also significantly decreased in SI females without a change in total VTA dopamine neurons (TH-positive) (Fig. 5B). In contrast, no significant changes were found on c-Fos-positive neurons in VTA of SI males (Fig. S3A). Another neuronal activity marker Egr1 gave similar results: decreased Egr1 expression level

Fig. 5 Social withdrawal in SI females is linked to the altered PFC to VTA pathway. A, **B** Confocal images and quantification of immunostaining of c-Fos (red), CaMKII (green) or TH (green), and DAPI (blue) in the PFC (**A**) or VTA (**B**) of GH and SI females (**A** $n = 12$ slice/4 mice/group, $t_{22} = 2.75$, $^{*}p < 0.05$, t test; **B** $n = 10$–13 slice/4 mice/group, $t_{24} = 5.52$, $^{***}p < 0.001$, t test). **C** Diagram and images showing the location and expression of the stereotaxically-injected GFP-Cre AAV to medial PFC and retrograde DIO-DREADD-mCherry AAV to female VTA. hM4D(Gi) DREADD was injected to GH females, while hM3D(Gq) DREADD was injected to SI females. The zoomed-in images of PFC show mCherry signals in GFP+ neurons, indicating that DREADD AAV is retro-transported from VTA to PFC. **D** Bar graphs showing the social interaction time during SA tests of GH females injected with saline or CNO to inhibit PFC → VTA pathway ($n = 7$/group, $t_{10} = 4.91$, $p < 0.001$, t test). **E** Bar graphs showing the social interaction time during SA tests of SI females injected with saline or CNO to activate PFC → VTA pathway ($n = 6$/group, $t_{10} = 2.53$, $p < 0.05$, t test). Data are presented as mean ± SEM. In all figures: $^{*}p < 0.05$; $^{**}p < 0.01$; $^{***}p < 0.001$.

in PFC and VTA of SI females (Fig. S3B, C), but not VTA of SI males (Fig. S3D). These data suggest that social isolation stress induces the dampening of PFC activity and the suppression of VTA activity in females.

To determine whether the alteration of PFC to VTA pathway is causally linked to antisocial behaviors in SI females, we next used the chemogenetic tool DREADD to manipulate this specific pathway in a bi-directional manner. The GFP-tagged Cre virus was injected bilaterally to PFC, and the mCherry-tagged retrograde double floxed DREADD virus was injected into the VTA of female mice. Gi DREADD was injected to VTA of GH females, and Gq DREADD was injected to VTA of SI females to examine the sufficiency and necessity of PFC to VTA pathway in sociability (Fig. 5C). We found that inhibiting PFC → VTA projection by CNO treatment in GH females induced marked social withdrawal during social approach tests (Fig. 5D), while activating PFC → VTA projection by CNO treatment in SI females significantly increased social interaction time (Fig. 5E). These data have provided bi-directional evidence indicating that PFC to VTA pathway is causally linked to female sociability.

Transcriptomic changes in VTA of stressed females underlie reduced sociability

To better understand how VTA is involved in isolation stress-induced female social withdrawal, we investigated transcriptomic changes of VTA in SI female mice. RNA-seq revealed 393 downregulated genes and 488 upregulated genes in the VTA of SI female mice, compared to VTA of GH females (Fig. 6A, Supplementary Tables 3, 4). Heatmaps of the down- and upregulated DEGs showed that GH samples clustered separately from SI samples (Fig. 6B). Functional annotation showed that down- and upregulated genes fell into the major categories including enzymes, signaling molecules, and transcription factors (Fig. 6C). GO analysis indicated that the most enriched biological process of downregulated genes was "neuropeptide signaling pathway" (Fig. 6D), while the upregulated genes were mainly involved in "synaptic signaling" (Fig. 6D).

Neuropeptide signaling pathway has been implicated in stress responses [48] and female-biased mental illness, such as depression [49, 50]. Interactome network indicated that neuropeptide genes *Hcrt*, *Pomc*, *Pmch* and *Tph2* were the "hubs" connecting with other top-ranking downregulated genes (Fig. 6E). Quantitative PCR confirmed the significant reduction of *Hcrt*, *Tph2*, and *Pomc* mRNAs in the VTA of SI female mice, compared to GH females (Fig. 6F). In contrast, none of these genes were significantly altered in SI male mice (Fig. 6G).

The top gene downregulated in VTA of SI females, *Hcrt*, encodes hypocretin (orexin), a neuropeptide regulating arousal, wakefulness, appetite, and endocrine homeostasis [51]. VTA is innervated by orexinergic neurons in lateral hypothalamus (Fig. 6H). Recently it has been found that orexin is especially critical for protecting against depressive reaction to stressful events [49]. So we tested whether elevating orexin levels in SI female mice could normalize the social behavior. Orexin A, a small peptide that specially binds to Orexin A receptor to activate orexin singling, was used to treat SI female mice (1 μmol/kg, i.p.). Immunohistochemical experiments showed that the number of c-Fos-positive dopamine neurons in the VTA of SI female mice was significantly increased after Orexin A treatment (Fig. 6I), indicating the restoration of VTA neuronal activity. In the social approach assay, Orexin A-treated SI females had significantly increased social interaction time than saline-treated SI females (Fig. 6J). These data suggest that Orexin A in females may serve as a potential therapeutic target for mental disorders related to social deficits.

DISCUSSION

In this study, we have used social isolation stress, an established stress paradigm for studying the neurobiology of mental illness [16, 17, 52]. Most of the prior social isolation studies were conducted in male subjects [13, 15, 18, 53, 54]. More current studies started to reveal the sex difference in stress responses [14, 55, 56]. Our results show that after 5 weeks of post-weaning social isolation, male mice exhibit heightened aggression, while female mice exhibit depression-like social withdrawal. It is in line with the sex difference in humans for stress-related mental disorders [4–7]. We have also found that stressed mice of both sexes share anxiety-like behaviors and schizophrenia-related sensorimotor gating impairment.

Excessive aggression is one of the common behavioral impairments associated with neuropsychiatric disorders, including anxiety and PTSD [57, 58]. The limbic system has been associated with the processing of emotionally salient events including aggression in human and animal studies [27, 32]. In particular, a major component of the limbic system, amygdala, is highly implicated in the processing of fear, defensive reactions, emotional learning, and motivation [22, 32]. BLA receives innervation from the prelimbic region of PFC [14, 25] and sends projections to the central amygdala to control fear and emotional responses [32]. Concomitant with heightened aggression in males subjected to chronic isolation stress, we have found the decreased neuronal activity in PFC and increased neuronal activity in BLA. The blockade of aggressive behaviors by chemogenetic activation of the PFC to BLA projections in stressed males further indicates the causal link of the PFC → BLA pathway to SI-induced aggression. Our optogenetic experiments suggest that the compromised PFC glutamatergic projections to BLA GABAergic interneurons cause disinhibition of BLA principal neurons and the switch of E/I balance towards excitation in BLA of SI male mice. It is consistent with recent findings on the central role of PFC activation and amygdala suppression in ameliorating pathological aggression [14, 59].

Social impairment is another common hallmark of neuropsychiatric diseases, including depression, schizophrenia, and autism. PFC and VTA are two crucial regions involved in the regulation of social behaviors [14, 21, 41, 42, 45–47]. Early life stress disrupts neuronal and synaptic functions of both PFC [14, 17, 60] and VTA [14, 20, 56]. The PFC to VTA projection controls the burst firing of DA neurons [61], and optogenetic studies have found that the enhanced phasic firing of VTA DA neurons mediates susceptibility to social defeat stress [21]. Our in vivo calcium imaging in behaving animals indicate that the reduced PFC activity is directly associated with the diminished social interaction in SI females. The amelioration of social withdrawal behaviors by chemogenetic

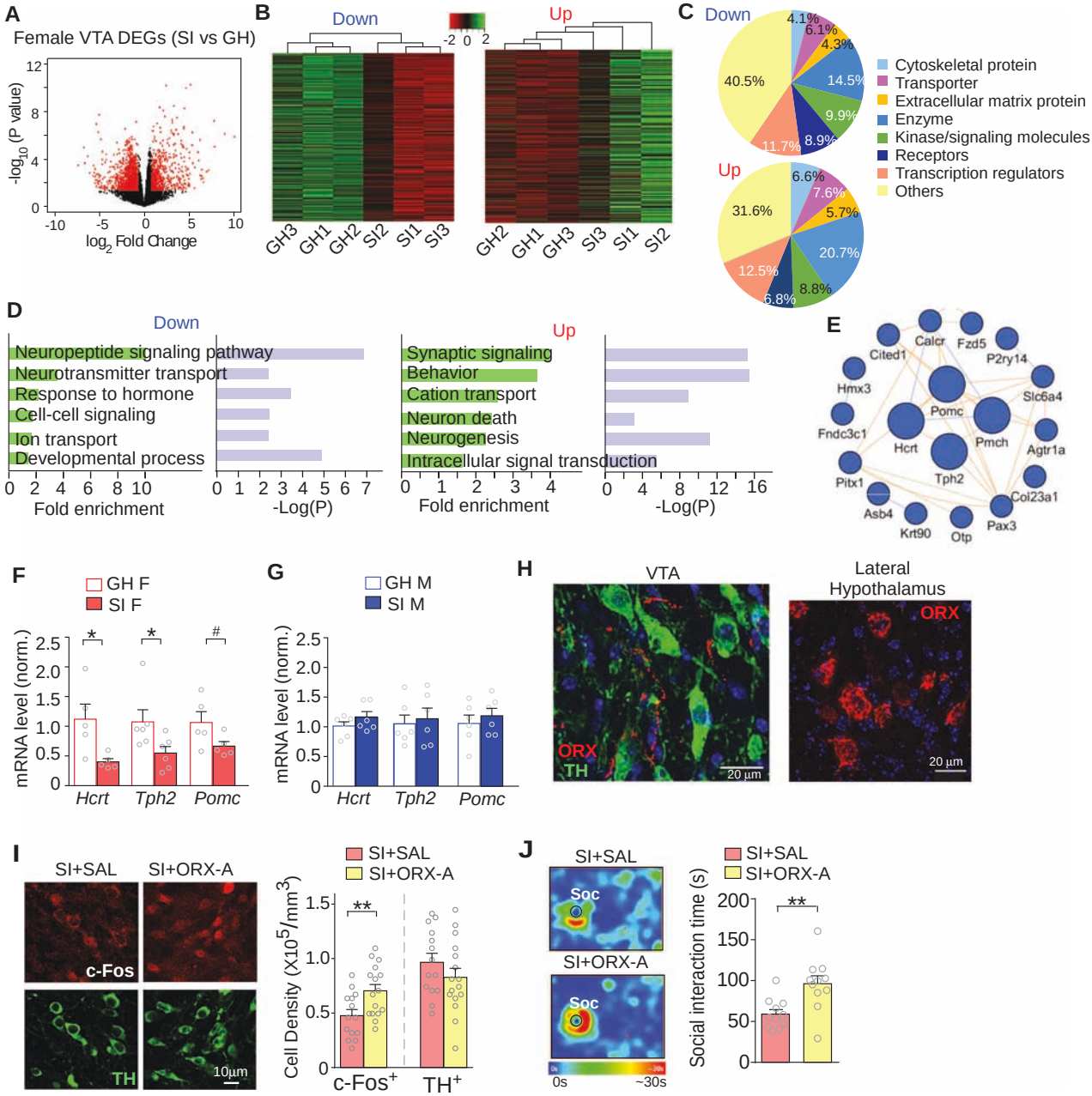

Fig. 6 Transcriptomic studies reveal the key role of VTA orexin signaling in female responses to isolation stress. A Volcano plot of differentially expressed genes in the VTA of SI females, compared to GH females. **B** Heatmaps of down- and upregulated genes in VTA of SI females, compared to GH controls. **C** Functional protein classification for the down- and upregulated genes. **D** Enrichment analysis for the down- and upregulated genes. **E** Protein-protein interaction (PPI) network of the top-ranking downregulated genes in VTA of SI females. Genes encoding neuropeptides, including *Hcrt, Pomc, Pmch* and *Tph2*, are hub genes of the PPI network. **F, G** Quantitative PCR data on the mRNA level of *Hcrt*, *Tph2* and *Pomc* in VTA of GH and SI female mice (**F**, $n = 5$/group, *Hcrt*: $p < 0.05$; *Tph2*: $p < 0.05$; *Pomc*: $p < 0.1$, *t* test) or VTA of GH and SI male mice (**G** $n = 6$/group). **H** Confocal images of immunostaining of Orexin A (red) and TH (green) in the VTA, and immunostaining of Orexin A (red) in the lateral hypothalamus. Blue: DAPI staining. **I** Confocal images and quantification of immunostaining of c-Fos (red) and TH (green) in the VTA of SI female mice treated with orexin A (ORX-A, 1 μmol/kg, i.p.) or saline (SAL) control ($n = 14$–16 slice from 3 mice/group, c-Fos: $t_{28} = 2.79$, $p < 0.01$, *t* test). **J** Bar graphs showing social interaction time during Social Approach tests of SI female mice treated with ORX-A or SAL ($n = 11$/group, $t_{20} = 3.34$, $p < 0.01$, *t* test). Insets: representative heatmaps illustrating the time spent in different locations of the apparatus during SA tests. Locations of social (Soc) stimuli are labeled with the circles. Data are presented as mean ± SEM. In all figures: #$p < 0.1$; *$p < 0.05$; **$p < 0.01$; ***$p < 0.001$.

activation of PFC to VTA projections in stressed females further demonstrates a crucial role of the PFC → VTA pathway in SI-induced social impairment.

PFC sends long-range monosynaptic inputs into VTA. VTA is composed of 65% dopaminergic neurons, 35% GABAergic neurons and 3–6% glutamatergic neurons [62]. Both dopaminergic and non-dopaminergic neurons receive PFC innervations [63]. These PFC-innervated neurons in VTA also shows divergent projections to other brain regions, such as PFC and NAc [63]. Changes in PFC → VTA pathway will alter dopamine release in target regions of VTA.

A puzzling question is why different neuronal regions are affected by stress in a sex-specific manner. We speculate that dysregulation of gene expression may underlie the different

physiological and behavioral changes observed in stressed animals. Our large-scale RNA-seq analyses have revealed region-specific transcriptomic alterations by isolation stress. Interestingly, the upregulated genes in BLA of SI males are enriched in the biological process of aggressive behaviors and are highly associated with the transcription factor CREB. CREB is activated by multiple kinase pathways [33], controls the transcription of many important genes, including c-fos, BDNF, TH, SST, VGF, corticotropin-releasing hormone, and has been implicated in the regulation of memory [64], emotional behaviors [36, 37], and affective disorders [38]. Here we show that the active form of CREB is increased in BLA of SI males, and inhibition of CREB is able to block the elevated aggressive behaviors, which offers a potential avenue for the treatment of stress-related aggression in males.

Another interesting finding from RNAseq is that many of the top-ranking downregulated genes in VTA of SI females are those involved in neuropeptide signaling implicated in stress responses and mental disorders [48–50], including *Hcrt*, *Pomc*, and *Tph2*. The top candidate *Hcrt*, which encodes hypocretin (orexin), plays a key role in regulating arousal and endocrine homeostasis [51], and is decreased in humans with depression, anxiety and PTSD [65–67]. Orexins have been found to mediate sex differences in cognitive flexibility [68], and promote stress resilience [49]. Here we show that activating orexin singling with Orexin A peptide to compensate for the loss of *Hcrt* expression in VTA of SI females could mitigate the social withdrawal behavior, pointing to orexins as a potential therapeutic target for treating stress-related social deficits in females.

The reason underlying stress-induced sex-specific transcriptional alterations is unclear. The prelimbic region of PFC contains anatomically and molecularly distinct subpopulations that target NAc, amygdala, and VTA [69]. NAc-projecting PFC neurons are found to be involved in the combined social and spatial coding [69], here we have revealed the link of BLA- or VTA-projecting PFC neurons to sex-specific behavioral changes by isolation stress. The up- or down-regulation of selective genes in BLA and VTA could be due to the cell type-specific activation of distinct transcription factors or chromatin regulators after chronic isolation stress in males and females.

Comparing to chronic social isolation stress, acute social isolation exerts a different effect on social behavior [70]. While chronic social isolation induces antisocial behaviors [14, 52], acute social isolation promotes social behaviors [71]. Sexually dimorphic neuronal responses to acute social isolation have also been reported. For example, less than 24 h social isolation decreases the excitability of PVN CRH neurons only in female mice [55]. Future studies are needed to find out how acute social isolation alters gene expression in different brain regions of both sexes.

Collectively, our data have revealed the role of region-specific molecular maladaptation in the behavioral manifestations of social isolation stress in male and female mice. Given the complexity of stress effects, the contribution of additional neural circuits and molecular pathways awaits further testing.

MATERIALS AND METHODS

Animals and chemicals

C57/BL6 mice and Emx1-IRES-Cre mice (Jackson Laboratory, stock #: 005628) were used in the study. As previously described [60], chronic adolescent social isolation (SI) was carried out after weaning from postnatal day 21 (P21) to P56 (5 weeks). Every 4 littermates were randomly divided into 1 socially-isolated (SI) mouse and 3 group-housed (GH) mice. Bedding and enrichment for SI and GH mice were the same. All animals were housed with ad libitum food accessibility in the 12 h light–dark cycle (light: 6 a.m.–6 p.m.; dark: 6 p.m.–-6 a.m.). Researchers were blind to group assignment and drug treatment during experiments. All animal studies were performed with the approval of the Institutional Animal Care and Use Committee of the State University of New York at Buffalo.

CREB inhibitor 666-15 (Tocris, Cat. # 5661) was dissolved in 1% N-methylpyrrolidone (NMP), 5% Tween-80 in H_2O. After 5-week social isolation stress, 666-15 or vehicle was stereotaxically delivered into the BLA at 1.6 mM, 0.5 µl/side [39, 40]. After 2-day recovery, animals were subject to behavioral tests, followed by brain tissue collection for qPCR. For p-CREB staining experiment, animals were sacrificed 6 h after 666-15 or vehicle delivery. Orexin-A (Tocris, Cat. # 1455) was dissolved in saline, i.p. injected at the dose of 1 µmol/kg, based on orexin-A pharmacokinetics [72]. Behavioral test was carried out 30 min after Orexin-A injection.

Behavior tests

See Supplementary Methods for details regarding behavioral assays, including Resident-intruder (RI), Elevated plus maze, Locomotion test, PPI, and Social approach.

Immunohistochemistry

See Supplementary Methods for details.

Chemogenetic study and animal surgery

The Cre-dependent adeno-associated virus AAV9-hSyn-HI-eGFP-Cre.WPRE.SV40 (1×10^{13} vg/ml) and the retrograde virus AAVrg-hSyn-DIO-hM4D(Gi)-mCherry (8×10^{12} vg/ml) or AAVrg-hSyn-DIO-hM3D(Gq)-mCherry (7×10^{12} vg/ml) were obtained from Addgene. Stereotaxic injections of the Cre virus into medial PFC (prelimbic and infralimbic, 0.5 µl), as well as the retrograde hM4Di or hM3Dq virus into BLA (0.5 µl) or VTA (0.5 µl), were performed as described previously [29]. In brief, mice were anesthetized (Ketamine [100 mg/kg] and Xylazine [5 mg/kg]) and placed on a stereotaxic apparatus (David Kopf Instruments). The injection was performed with a Hamilton syringe (needle gauge 31) at a speed of 0.1 µl/min, and the needle was kept in place for an additional 5 min. The virus was delivered bilaterally to the target area using the following coordinates: PFC: 1.98 mm anterior to bregma; 0.25 mm lateral; and 2.2 mm dorsal to ventral; BLA: 1.46 mm posterior to bregma; 2.8 mm lateral; and 4.9 mm dorsal to ventral; VTA: 3.64 mm posterior to bregma; 0.5 mm lateral; and 4.2 mm dorsal to ventral. All behavioral tests were conducted 3 weeks after surgery. Behavioral testing was performed 1–4 h after intraperitoneal injection of CNO or saline in viral-infected mice. Fluorescence images were taken on a Leica DMI8 inverted microscope.

Optogenetic and electrophysiological study

AAV9-CaMKII-hChR2-mCherry (1×10^{13} vp/ml, Addgene) was injected into the PFC of mice. After 5 weeks of virus expression, animals were sacrificed for whole-cell voltage-clamp recording, as previously described [25, 30]. Mice were anesthetized with Halothane (Sigma) inhalation. Brains were immediately removed, iced and cut into 300 µm slices by a Vibratome (Leica VP1000S). Mouse brain slices were then positioned in a perfusion chamber attached to the fixed stage of an upright microscope (Olympus) and submerged in continuously flowing oxygenated ACSF (in mM: 130 NaCl, 26 $NaHCO_3$, 3 KCl, 5 $MgCl_2$, 1.25 NaH_2PO_4, 1 $CaCl_2$, 10 Glucose, pH 7.4, 300 mOsm). Light stimulation of ChR2-expressing terminals in BLA slices was carried out using a UHP-Microscope-LED-460 system (Prizmatix) that provides >1 W collimated blue light (460 nm peak, 27 nm spectrum half-width, 85% peak power at 450 nm). The blue light was transmitted via the microscope objective (Olympus LUMPlanFI/IR, 40 × 0.80w) and triggered on and off with TTL pulses programmed by pClamp data acquisition software (Molecular Devices, Sunnyvale, CA). The LED output power control of Prizmatix UHP-LED controller was set at 10 and the blue pulse stimulation duration was 5 ms.

To demonstrate the effect of stimulating PFC inputs on BLA neuronal response, inhibitory and excitatory postsynaptic currents evoked by light stimulation (Opto-IPSC, Opto-EPSC) in BLA principal neurons (identified by the large soma size) were recorded. Electrode internal solution was composed of (in mM): 130 Cs-methanesulfonate, 3 CsCl, 4 NaCl, 10 HEPES, 5 EGTA, 1 $MgCl_2$, 4 MgATP, 0.3 NaGTP, 5 QX314 (pH 7.2, 290 mOsm). Based on the external and internal ion concentrations of recording conditions, the reversal potential of $GABA_A$ receptor channels was calculated at −70 mV, and the reversal potential of glutamate receptor channels was at ~0 mV. Opto-IPSC and Opto-EPSC were recorded at 0 mV and −70 mV, respectively. Data were acquired using the software pClamp 9.2 (Molecular Devices). The data sampling frequency was 10 kHz, and the filtering frequency was 1 kHz. Data analyses were performed with the Clampfit software (Molecular Devices).

In vivo calcium imaging of behaving animals

AAV5.Syn.Flex.GCaMP6s.WPRE.SV40 virus (7×10^{12} vp/ml, Addgene, 100845-AAV5) was injected into the PFC of female Emx1-IRES-Cre mice. After 4 weeks of virus expression, a 400 µm-diameter 0.50-NA fiber (Thorlabs, FP400ERT) was surgically implanted above the PFC. The GCaMP6s fluorescence was alternatively excited by a 470-nm LED with 470/10 nm bandpass and a 410-nm LED with 410/10 nm bandpass. The LEDs (Thorlabs) were switched at 100 Hz. When GCaMP6s is excited at 470 nm, the emitted fluorescence intensity is Ca^{2+} sensitive, but when it is excited at 410 nm, the emission is largely Ca^{2+} insensitive, which was used as a control for motion artifacts. The excitation light was reflected off a 495 nm longpass dichroic mirror (Semrock, FF495-Di02-25 × 36) and focused by a 20× objective lens (0.4 NA; Olympus) into a custom-made low optical fiber (400 µm, Thorlabs) that guided the light to the optical fiber implanted in the brain. The fluorescence emission signal was filtered through a 520 nm bandpass fluorescence filter (Semrock, FF01-520/35-25) and focused on a small spot on an ANDOR sCMOS camera. The data was recorded at 100 Hz, which after deconvoluting the Ca^{2+} signal from the isosbestic control, resulted in a temporal resolution of 50 ms. All the data were processed and analyzed in Image J and IgorPro 8.0.

RNA-sequencing and bioinformatic analysis

After animal sacrificing, brain tissues were sliced with a 1 mm brain matrix (Zivic Instruments, Pittsburgh, PA). Then brain punches containing BLA or VTA areas were collected using a puncher (diameter: 2 mm). As previously described [24], total RNA was isolated from BLA and VTA samples obtained from group-housed and isolation-stressed male and female mice using the RNAeasy Mini kit (Qiagen), coupled to an RNase-free DNase step (Qiagen). The RNA-sequencing libraries were constructed by TruSeq stranded total RNA plus Ribo-zero kits (Illumina). Sequencing was carried out with the HiSeq 2500 platform (Illumina) at the Genomics and Bioinformatics Core of the State University of New York at Buffalo. RNA-seq tags reads were aligned to the mouse GRCm38-mm10 RefSeq mRNAs using TopHat2 with default parameters. In GRCm38-mm10, all of the 20,423 component sequences were applied in Mapping and Annotation. Alignments with a mapping score <10 were discarded using SAMtools. Feature Counts was used to generate a matrix of mapped fragments per USCS RefSeq known annotated gene, from which genes annotated by RefSeq as rRNA were discarded. Full threshold-free differential expression was detected by edgeR. The GLM (generalized linear model) in the edgeR package was used. Assuming that an estimate is available for ϕ_{gi}, so the variance can be evaluated for any value of μ_{gi}, GLM theory can be used to fit a log-linear model, $\log \mu_{gi} = X_i^T \beta_g + \log N_i$, where X_i is a vector of covariates that specifies the treatment conditions applied to RNA sample i, and β_g is a vector of regression coefficients by which the covariate effects are mediated for gene g. The differentially expressed genes were defined with at least 1.2-Fold Change (FC) and $P < 0.05$. Functional protein classification analyses were undertaken using Panther. Enrichment analyses of differentially expressed genes were conducted using gene sets derived from the Biological Process Ontology from DAVID (https://david.ncifcrf.gov/). Gene set enrichment analysis (GSEA) was undertaken using GSEA software [73]. Full threshold-free differential expression lists were ranked by the −log10 (*p* value) multiplied by the sign of the fold change from the edgeR analysis.

Western blotting

See Supplementary Methods for details.

Quantitative real-time RT-PCR

Primers for all the target genes are listed in Supplementary Table 5. See Supplementary Methods for details.

Statistics

All statistical analyses were performed with Graphpad Prism and Minitab 18. Sample sizes were determined based on power analyses and were similar to those reported in previous works [24, 25, 29, 30]. Experiments with more than two groups were subjected to two-way ANOVA with Bonferroni correction for multiple post hoc comparisons. Experiments with two groups were analyzed statistically using two-tailed unpaired *t* tests. All data are presented as the mean ± SEM. Data points identified as statistically significant outliers (determined by Grubb's test, $p < 0.05$) were removed from the analyses. The variance between groups being statistically compared was similar.

DATA AVAILABILITY

All data needed to evaluate the conclusions in the paper are present in the paper and/or the Supplementary Materials. The RNA-seq data generated in this study have been deposited in the GEO public repository under accession code GSE198725.

REFERENCES

1. Sanacora G, Yan Z, Popoli M. The stressed synapse 2.0: pathophysiological mechanisms in stress-related neuropsychiatric disorders. Nat Rev Neurosci. 2022;23:86–103.
2. McEwen BS, Bowles NP, Gray JD, Hill MN, Hunter RG, Karatsoreos IN, et al. Mechanisms of stress in the brain. Nat Neurosci. 2015;18:1353–63.
3. Archer J. Sex differences in aggression between heterosexual partners: a meta-analytic review. Psychol Bull. 2000;126:651.
4. Kessler RC. Epidemiology of women and depression. J Affect Disord. 2003;74:5–13.
5. Kornstein SG, Schatzberg AF, Thase ME, Yonkers KA, McCullough JP, Keitner GI, et al. Gender differences in chronic major and double depression. J Affect Disord. 2000;60:1–11.
6. Breslau N, Davis GC, Andreski P, Peterson EL, Schultz LR. Sex differences in posttraumatic stress disorder. Arch Gen Psychiatry. 1997;54:1044–8.
7. Tolin DF, Foa EB. Sex differences in trauma and posttraumatic stress disorder: a quantitative review of 25 years of research. Psychol Bull. 2006;132:959–92.
8. Yan Z, Rein B. Mechanisms of synaptic transmission dysregulation in the prefrontal cortex: pathophysiological implications. Mol Psychiatry. 2021. https://doi.org/10.1038/s41380-021-01092-3.
9. Spear LP. The adolescent brain and age-related behavioral manifestations. Neurosci Biobehav Rev. 2000;24:417–63.
10. Walker DM, Cunningham AM, Gregory JK, Nestler EJ. Long-term behavioral effects of post-weaning social isolation in males and females. Front Behav Neurosci. 2019;13:66.
11. Lupien SJ, McEwen BS, Gunnar MR, Heim C. Effects of stress throughout the lifespan on the brain, behaviour and cognition. Nat Rev Neurosci. 2009;10:434–45.
12. Paus T, Keshavan M, Giedd JN. Why do many psychiatric disorders emerge during adolescence? Nat Rev Neurosci. 2008;9:947–57.
13. Wongwitdecha N, Marsden CA. Social isolation increases aggressive behaviour and alters the effects of diazepam in the rat social interaction test. Behav Brain Res. 1996;75:27–32.
14. Tan T, Wang W, Liu T, Zhong P, Conrow-Graham M, Tian X, et al. Neural circuits and activity dynamics underlying sex-specific effects of chronic social isolation stress. Cell Rep. 2021;34:108874.
15. Amiri S, Haj-Mirzaian A, Rahimi-Balaei M, Razmi A, Kordjazy N, Shirzadian A, et al. Co-occurrence of anxiety and depressive-like behaviors following adolescent social isolation in male mice; possible role of nitrergic system. Physiol Behav. 2015;145:38–44.
16. Van den Berg CL, Pijlman FT, Koning HA, Diergaarde L, Van Ree JM, Spruijt BM. Isolation changes the incentive value of sucrose and social behaviour in juvenile and adult rats. Behav Brain Res. 1999;106:133–42.
17. Liu J, Dietz K, DeLoyht JM, Pedre X, Kelkar D, Kaur J, et al. Impaired adult myelination in the prefrontal cortex of socially isolated mice. Nat Neurosci. 2012;15:1621–3.
18. Han X, Wang W, Xue X, Shao F, Li N. Brief social isolation in early adolescence affects reversal learning and forebrain BDNF expression in adult rats. Brain Res Bull. 2011;86:173–8.
19. Wang YC, Ho UC, Ko MC, Liao CC, Lee LJ. Differential neuronal changes in medial prefrontal cortex, basolateral amygdala and nucleus accumbens after post-weaning social isolation. Brain Struct Funct. 2012;217:337–51.
20. Pena CJ, Kronman HG, Walker DM, Cates HM, Bagot RC, Purushothaman I, et al. Early life stress confers lifelong stress susceptibility in mice via ventral tegmental area OTX2. Science. 2017;356:1185–8.
21. Chaudhury D, Walsh JJ, Friedman AK, Juarez B, Ku SM, Koo JW, et al. Rapid regulation of depression-related behaviours by control of midbrain dopamine neurons. Nature. 2013;493:532–6.
22. Gold PW. The organization of the stress system and its dysregulation in depressive illness. Mol Psychiatry. 2015;20:32–47.
23. Fone KC, Porkess MV. Behavioural and neurochemical effects of post-weaning social isolation in rodents-relevance to developmental neuropsychiatric disorders. Neurosci Biobehav Rev. 2008;32:1087–102.
24. Wang ZJ, Zhong P, Ma K, Seo JS, Yang F, Hu Z, et al. Amelioration of autism-like social deficits by targeting histone methyltransferases EHMT1/2 in Shank3-deficient mice. Mol Psychiatry. 2020;25:2517–33.
25. Wei J, Zhong P, Qin L, Tan T, Yan Z. Chemicogenetic restoration of the prefrontal cortex to amygdala pathway ameliorates stress-induced deficits. Cereb Cortex. 2018;28:1980–90.

26. Rapanelli M, Tan T, Wang W, Wang X, Wang ZJ, Zhong P, et al. Behavioral, circuitry, and molecular aberrations by region-specific deficiency of the high-risk autism gene Cul3. Mol Psychiatry. 2021;26:1491–504.
27. Davidson RJ, Putnam KM, Larson CL. Dysfunction in the neural circuitry of emotion regulation-a possible prelude to violence. Science. 2000;289:591–4.
28. Arruda-Carvalho M, Clem RL. Pathway-selective adjustment of prefrontal-amygdala transmission during fear encoding. J Neurosci. 2014;34:15601–9.
29. Wang W, Rein B, Zhang F, Tan T, Zhong P, Qin L, et al. Chemogenetic activation of prefrontal cortex rescues synaptic and behavioral deficits in a mouse model of 16p11.2 deletion syndrome. J Neurosci. 2018;38:5939–48.
30. Zhong P, Qin L, Yan Z. Dopamine differentially regulates response dynamics of PFC principal neurons and interneurons to optogenetic stimulation of VTA inputs. Cereb Cortex. 2020;30:4402–9.
31. Nelson RJ, Trainor BC. Neural mechanisms of aggression. Nat Rev Neurosci. 2007;8:536–46.
32. Cardinal RN, Parkinson JA, Hall J, Everitt BJ. Emotion and motivation: the role of the amygdala, ventral striatum, and prefrontal cortex. Neurosci Biobehav Rev. 2002;26:321–52.
33. Wu GY, Deisseroth K, Tsien RW. Activity-dependent CREB phosphorylation: convergence of a fast, sensitive calmodulin kinase pathway and a slow, less sensitive mitogen-activated protein kinase pathway. Proc Natl Acad Sci USA. 2001;98:2808–13.
34. Boer U, Alejel T, Beimesche S, Cierny I, Krause D, Knepel W, et al. CRE/CREB-driven up-regulation of gene expression by chronic social stress in CRE-luciferase transgenic mice: reversal by antidepressant treatment. PLoS ONE. 2007;2:e431.
35. Yin JC, Wallach JS, Del Vecchio M, Wilder EL, Zhou H, Quinn WG, et al. Induction of a dominant negative CREB transgene specifically blocks long-term memory in Drosophila. Cell. 1994;79:49–58.
36. Valverde O, Mantamadiotis T, Torrecilla M, Ugedo L, Pineda J, Bleckmann S, et al. Modulation of anxiety-like behavior and morphine dependence in CREB-deficient mice. Neuropsychopharmacology. 2004;29:1122–33.
37. Barrot M, Wallace DL, Bolanos CA, Graham DL, Perrotti LI, Neve RL, et al. Regulation of anxiety and initiation of sexual behavior by CREB in the nucleus accumbens. Proc Natl Acad Sci USA. 2005;102:8357–62.
38. Blendy JA. The role of CREB in depression and antidepressant treatment. Biol Psychiatry. 2006;59:1144–50.
39. Xie F, Li BX, Kassenbrock A, Xue C, Wang X, Qian DZ, et al. Identification of a potent inhibitor of CREB-mediated gene transcription with efficacious in vivo anticancer activity. J Med Chem. 2015;58:5075–87.
40. Li BX, Gardner R, Xue C, Qian DZ, Xie F, Thomas G, et al. Systemic inhibition of CREB is well-tolerated in vivo. Sci Rep. 2016;6:34513.
41. Franklin TB, Silva BA, Perova Z, Marrone L, Masferrer ME, Zhan Y, et al. Prefrontal cortical control of a brainstem social behavior circuit. Nat Neurosci. 2017;20:260–70.
42. Qin L, Ma K, Wang ZJ, Hu Z, Matas E, Wei J, et al. Social deficits in Shank3-deficient mouse models of autism are rescued by histone deacetylase (HDAC) inhibition. Nat Neurosci. 2018;21:564–75.
43. Kim CK, Yang SJ, Pichamoorthy N, Young NP, Kauvar I, Jennings JH, et al. Simultaneous fast measurement of circuit dynamics at multiple sites across the mammalian brain. Nat Methods. 2016;13:325–8.
44. Chen TW, Wardill TJ, Sun Y, Pulver SR, Renninger SL, Baohan A, et al. Ultrasensitive fluorescent proteins for imaging neuronal activity. Nature. 2013;499:295–300.
45. Gunaydin LA, Grosenick L, Finkelstein JC, Kauvar IV, Fenno LE, Adhikari A, et al. Natural neural projection dynamics underlying social behavior. Cell. 2014;157:1535–51.
46. Bariselli S, Tzanoulinou S, Glangetas C, Prevost-Solie C, Pucci L, Viguie J, et al. SHANK3 controls maturation of social reward circuits in the VTA. Nat Neurosci. 2016;19:926–34.
47. Hung LW, Neuner S, Polepalli JS, Beier KT, Wright M, Walsh JJ, et al. Gating of social reward by oxytocin in the ventral tegmental area. Science. 2017;357:1406–11.
48. Kash TL, Pleil KE, Marcinkiewcz CA, Lowery-Gionta EG, Crowley N, Mazzone C, et al. Neuropeptide regulation of signaling and behavior in the BNST. Mol Cells. 2015;38:1–13.
49. Ji MJ, Zhang XY, Chen Z, Wang JJ, Zhu JN. Orexin prevents depressive-like behavior by promoting stress resilience. Mol Psychiatry. 2019;24:282–93.
50. Grippo AJ, Gerena D, Huang J, Kumar N, Shah M, Ughreja R, et al. Social isolation induces behavioral and neuroendocrine disturbances relevant to depression in female and male prairie voles. Psychoneuroendocrinology. 2007;32:966–80.
51. de Lecea L, Kilduff TS, Peyron C, Gao X, Foye PE, Danielson PE, et al. The hypocretins: hypothalamus-specific peptides with neuroexcitatory activity. Proc Natl Acad Sci USA. 1998;95:322–7.
52. Zelikowsky M, Hui M, Karigo T, Choe A, Yang B, Blanco MR, et al. The neuropeptide Tac2 controls a distributed brain state induced by chronic social isolation stress. Cell. 2018;173:1265–79.e19.
53. Mikics E, Guirado R, Umemori J, Toth M, Biro L, Miskolczi C, et al. Social learning requires plasticity enhanced by fluoxetine through prefrontal Bdnf-TrkB signaling to limit aggression induced by post-weaning social isolation. Neuropsychopharmacology. 2018;43:235–45.
54. Toth M, Mikics E, Tulogdi A, Aliczki M, Haller J. Post-weaning social isolation induces abnormal forms of aggression in conjunction with increased glucocorticoid and autonomic stress responses. Horm Behav. 2011;60:28–36.
55. Senst L, Baimoukhametova D, Sterley TL, Bains JS. Sexually dimorphic neuronal responses to social isolation. Elife. 2016;5:e18726.
56. Pena CJ, Smith M, Ramakrishnan A, Cates HM, Bagot RC, Kronman HG, et al. Early life stress alters transcriptomic patterning across reward circuitry in male and female mice. Nat Commun. 2019;10:5098.
57. Neumann ID, Veenema AH, Beiderbeck DI. Aggression and anxiety: social context and neurobiological links. Front Behav Neurosci. 2010;4:12.
58. Aleyasin H, Flanigan ME, Russo SJ. Neurocircuitry of aggression and aggression seeking behavior: nose poking into brain circuitry controlling aggression. Curr Opin Neurobiol. 2018;49:184–91.
59. van Heukelum S, Tulva K, Geers FE, van Dulm S, Ruisch IH, Mill J, et al. A central role for anterior cingulate cortex in the control of pathological aggression. Curr Biol. 2021;31:2321–33.e5.
60. Yamamuro K, Yoshino H, Ogawa Y, Makinodan M, Toritsuka M, Yamashita M, et al. Social isolation during the critical period reduces synaptic and intrinsic excitability of a subtype of pyramidal cell in mouse prefrontal cortex. Cereb Cortex. 2018;28:998–1010.
61. Murase S, Grenhoff J, Chouvet G, Gonon FG, Svensson TH. Prefrontal cortex regulates burst firing and transmitter release in rat mesolimbic dopamine neurons studied in vivo. Neurosci Lett. 1993;157:53–6.
62. Holly EN, Miczek KA. Ventral tegmental area dopamine revisited: effects of acute and repeated stress. Psychopharmacology. 2016;233:163–86.
63. Carr DB, Sesack SR. Projections from the rat prefrontal cortex to the ventral tegmental area: target specificity in the synaptic associations with mesoaccumbens and mesocortical neurons. J Neurosci. 2000;20:3864–73.
64. Zamarbide M, Mossa A, Munoz-Llancao P, Wilkinson MK, Pond HL, Oaks AW, et al. Male-specific cAMP signaling in the hippocampus controls spatial memory deficits in a mouse model of autism and intellectual disability. Biol Psychiatry. 2019;85:760–8.
65. Brundin L, Bjorkqvist M, Petersen A, Traskman-Bendz L. Reduced orexin levels in the cerebrospinal fluid of suicidal patients with major depressive disorder. Eur Neuropsychopharmacol. 2007;17:573–9.
66. Johnson PL, Truitt W, Fitz SD, Minick PE, Dietrich A, Sanghani S, et al. A key role for orexin in panic anxiety. Nat Med. 2010;16:111–5.
67. Strawn JR, Pyne-Geithman GJ, Ekhator NN, Horn PS, Uhde TW, Shutter LA, et al. Low cerebrospinal fluid and plasma orexin-A (hypocretin-1) concentrations in combat-related posttraumatic stress disorder. Psychoneuroendocrinology. 2010;35:1001–7.
68. Grafe LA, Cornfeld A, Luz S, Valentino R, Bhatnagar S. Orexins mediate sex differences in the stress response and in cognitive flexibility. Biol Psychiatry. 2017;81:683–92.
69. Murugan M, Jang HJ, Park M, Miller EM, Cox J, Taliaferro JP, et al. Combined social and spatial coding in a descending projection from the prefrontal cortex. Cell. 2017;171:1663–77.e16.
70. Lee CR, Chen A, Tye KM. The neural circuitry of social homeostasis: consequences of acute versus chronic social isolation. Cell. 2021;184:2794–5.
71. Matthews GA, Nieh EH, Vander Weele CM, Halbert SA, Pradhan RV, Yosafat AS, et al. Dorsal raphe dopamine neurons represent the experience of social isolation. Cell. 2016;164:617–31.
72. Ehrstrom M, Naslund E, Levin F, Kaur R, Kirchgessner AL, Theodorsson E, et al. Pharmacokinetic profile of orexin A and effects on plasma insulin and glucagon in the rat. Regul Pept. 2004;119:209–12.
73. Subramanian A, Tamayo P, Mootha VK, Mukherjee S, Ebert BL, Gillette MA, et al. Gene set enrichment analysis: a knowledge-based approach for interpreting genome-wide expression profiles. Proc Natl Acad Sci USA. 2005;102:15545–50.

ACKNOWLEDGEMENTS

We thank Xiaoqing Chen and Kaijie Ma for their excellent technical support. We also thank the support of the Genomics and Bioinformatics Core of the State University of New York at Buffalo. This work was supported by grants from the National Institutes of Health (R01-MH108842 and R01-MH126443 to ZY, R01-MH111872 to AP and K01-DA050908 to ZJW).

AUTHOR CONTRIBUTIONS

ZJW performed behavioral, immunohistochemical, biochemical, and molecular biological experiments, analyzed data, and wrote the paper; TS performed DREADD experiments and analyzed data. JL and AP designed and performed calcium imaging experiments and analyzed data. PZ performed optogenetic and electrophysiological experiments and analyzed data. FY analyzed genomic data. KS performed some immunohistochemical experiments. FZ performed some behavioral and biochemical experiments. ZY designed experiments, supervised the project, and wrote the paper.

COMPETING INTERESTS

The authors declare no competing interests.

ADDITIONAL INFORMATION

Supplementary information The online version contains supplementary material available at https://doi.org/10.1038/s41380-022-01574-y.

Correspondence and requests for materials should be addressed to Zhen Yan.

Reprints and permission information is available at http://www.nature.com/reprints

Publisher's note Springer Nature remains neutral with regard to jurisdictional claims in published maps and institutional affiliations.